Separation energy dependence of hole form factors in a simple microscopic model

H. Langevin-Joliot and J. Van de Wiele
Institut de Physique Nucléaire, IN2P3-CNRS-UniversitParis-Sud Orsay, France
(July 8, 2003)

Form factor of fragmented neutron hole states in ^{207}Pb are studied via microscopic calculations in the limiting case of incoherent contributions of hole coupling with two hole one particle states. The calculations were performed using the inhomogeneous equation method with a Serber-exponential nucleon nucleon effective force. Large fluctuations of form factor radii deduced for individual levels are observed. The role of the level configurations and of the nucleon nucleon force parameters are discussed in details in the case of $g_{7/2}$ inner hole fragments. The underlying dependences of form factor radii on separation energy deduced for the different valence and inner hole states are found much smaller than predicted in the framework of the quasiparticle-phonon model (QPM). This difference is qualitatively related to larger contributions of transition densities at smaller radii, compared with the strong surface localization of collective transitions involved in QPM calculations. The consequences on pick-up cross section analyses and spectroscopic factors of the rather small form factor radius dependences deduced in the present calculations are evaluated in the case of the $(\vec{d},t)$ reaction on ^{208}Pb at E$_d$=200 MeV.

EXT-2003-069
22/09/2003

I. INTRODUCTION

Most results on the fragmentation of hole states rely on the analysis of pick-up reactions performed with unpolarized and also polarized beams. Fragment form factors entering such analyses are generally derived using the simple well depth procedure, which only provides a correct description of the fragment wave function tails, but not of their internal parts. It has long been recognized that such an approximation may induce significant errors on the extraction of spectroscopic factors for fragments located several MeV away from the pure state.

The complexity of form factor theories developed as a more general approach of nuclear structure calculations [1], has prevented their use for practical purposes, except in very few cases. For example, a few particle-vibration coupling states in odd nuclei around ^{208}Pb have been calculated by Hamamoto [2] by solving a set of coupled differential equations. The admixed single-particle wave function of each of such fragments is bound at the correct energy. Formally, the coupling strength being known, these wave functions are solutions of inhomogeneous differential equations obtained from the Schrodinger equation. Austern [3] has proposed to skip the solution of the coupled equations and concentrate on the prediction of the sole shape of the inhomogeneous term via a structure calculation. The right hand side of such equation (hereafter the source term) would not change much by using pure single-particle radial functions in its calculation, instead of radial functions resulting of coupled equations.

We had used the inhomogeneous equation method in Ref. [4] to address the question of form factors in the framework of the quasiparticle-phonon model (hereafter QPM) [5]. Hole states in the doubly magic nucleus ^{208}Pb were discussed for practical examples. The large fluctuations of form factor radii deduced for the fragments of each $n\ell j$ hole state were found to be superimposed over a smooth and quite significant increase with separation energy. This important feature was taken into account in the analysis of neutron hole fragmentation in ^{208}Pb [6] and $^{116,120}Sn$ [7], studied via the $(\vec{d},t)$ reaction at E$_d$=200 MeV.

The strong separation energy dependence of hole form factors predicted with the QPM model is induced by the surface localization of the collective interaction, assumed to be of Woods-Saxon derivative shape. A further step would be to take into account the excited level transition densities.

A more fundamental microscopic approach, starting with an effective nucleon-nucleon interaction, would need in principle a correct description of the core states in term of superpositions of one particle-one hole configurations (and higher order configurations) together with inclusion of the Pauli principle constraints.

It seemed to us interesting to investigate the separation energy dependence of hole form factors in the case of a description of the underlying core excited states drastically opposite to the collective approach. In the present paper, we describe the core states as sets of pure particle-hole states of different spins and parities. Neutron hole form factors and form factor radii in ^{207}Pb are calculated within this very schematic assumption, for a large set of hole fragments resulting of the hole coupling with pure two hole-one particle states induced by an effective nucleon-nucleon interaction. .

The general formalism used in the present form factor calculations is described in Sect. II. The method, the assumptions adopted in the calculation of hole form factors in ^{207}Pb and the results are presented in Sect. III . Source terms and form factor radii are discussed in details in the case of $g_{7/2}$ levels. Spectroscopic factor analysis in the $(\vec{d},t)$ reaction at 200 MeV, taking into account form factors obtained either in the present calculations or in the frame-work of the QPM model is discussed in Sect. IV. Summary and conclusions are given in Sect. V.

II. GENERAL FORMALISM OF FORM FACTOR MICROSCOPIC CALCULATIONS

The Hamiltonian of the system of A-1 nucleons is separated into three parts, as given by Eq. 1

$$H = H_A + H_h + H_{int} \tag{1}$$

where H_A is the Hamiltonian for the internal motion of the core, H_h is that of the hole and H_{int} expresses the interaction between the odd particle (hole) and the core.

The internal motion of the core is described as a particle-hole excitation (hereafter p-h excitation), the hole being coupled to the two hole-one particle state (hereafter 2h1p state) via a central nucleon-nucleon interaction. Under those conditions, the total wave function is given by Eq. 2.

$$|\Psi^{M}_{J}> = \frac{1}{r}\Big\{\mathcal{R}_{\ell_1 j_1}(r)\; i^{\ell_1}\{[Y_{\ell_1}\chi_{1/2}]_{j_1}\Phi_{J_1}\}^{M}_{J} + \mathcal{R}_{\ell_2 j_2}(r)\; i^{\ell_2}\{[Y_{\ell_2}\chi_{1/2}]_{j_2}\Phi_{J_2}\}^{M}_{J}\Big\} \tag{2}$$

where $\mathcal{R}_{\ell_1 j_1}(r)/r$ is the form factor of the hole coupled to the core ground state with spin zero and $\mathcal{R}_{\ell_2 j_2}(r)/r$ is the form factor of the hole coupled to the excited particle-hole state with the wave function Φ_{J_2}. The total angular momentum of the considered hole fragment and the total angular momentum of the p-h excitation are J and J_2 respectively . We are interested in the form factor of the hole with no excitation of the core.

The corresponding radial wave functions $\mathcal{R}_{\ell_1 j_1}(r)$ are solutions of two coupled equations. In the case of the fragment with the smallest amplitude, the radial function is well approximated by solving the inhomogeneous equation 3.

$$\left\{\frac{d^2}{dr^2} - \frac{\ell_1(\ell_1+1)}{r^2} - \frac{2\mathcal{M}}{\hbar^2}V_{\ell_1 j_1}(r) + \frac{2\mathcal{M}}{\hbar^2}E\right\}\mathcal{R}_{\ell_1 j_1}(r) = S(r) \tag{3}$$

where the source term S(r)is

$$S(r) = \frac{2\mathcal{M}}{\hbar^2}\; i^{\ell_2-\ell_1} \;< \{[Y_{\ell_1}\chi_{1/2}]_{j_1}\Phi_{J_1}\}^{M}_{J}|H_{\rm int}|\{[Y_{\ell_2}\chi_{1/2}]_{j_2}\Phi_{J_2}\}^{M}_{J} > x_2\; \mathcal{R}_{n_2\ell_2 j_2}(r) \tag{4}$$

Here $\mathcal{R}_{\ell_2 j_2}(r)/r$, the exact radial function solution of Eq. 2 is approximated by the normalized solution of the Schrodinger equation 5 multiplied by the amplitude x_2 determined by a diagonalization procedure.

$$\left\{\frac{d^2}{dr^2} - \frac{\ell_2(\ell_2+1)}{r^2} - \frac{2\mathcal{M}}{\hbar^2}V_{\ell_2 j_2}(r) + \frac{2\mathcal{M}}{\hbar^2}\mathcal{E}_{n_2\ell_2 j_2}\right\}\mathcal{R}_{n_2\ell_2 j_2}(r) = 0. \tag{5}$$

The coupling matrix element is expressed in Eq. 6.

$$\begin{aligned}
& i^{\ell_2-\ell_1} \;< \{[Y_{\ell_1}\chi_{1/2}]_{j_1}\Phi_{J_1}\}^{M}_{J}|H_{\rm int}|\{[Y_{\ell_2}\chi_{1/2}]_{j_2}\Phi_{J_2}\}^{M}_{J} > \\
&= \sum_{\ell_{tr} j_{tr} \Sigma}\; i^{\ell_2-\ell_{tr}-\ell_1}\;\; (-1)^{j_{tr}+J-j_2-J_1}\;\;\hat{j}_1\;\hat{J}_1\;\; W(j_2 j_1 J_2 J_1; j_{tr} J) \\
& (-1)^{\Sigma}\;\hat{\Sigma}\;\sqrt{2}\;\;\hat{j_{tr}}\;\;\hat{j}_2\;\;\hat{\ell_{tr}}\;\;\hat{\ell}_2\;\;\frac{<\ell_2 0\ell_{tr}00|\ell_1 0>}{\sqrt{4\pi}}\;\left\{\begin{array}{ccc}\ell_1 & 1/2 & j_1\\ \ell_{tr} & \Sigma & j_{tr}\\ \ell_2 & 1/2 & j_2\end{array}\right\} \\
& \sum_{\ell_{p'} j_{p'} \ell_{h'} j_{h'}}\;\; i^{\ell_{tr}+\ell_{h'}-\ell_{p'}}\;\;(-1)^{j_{h'}-j_{p'}+j_{tr}}\;\;\hat{j}_{p'}\;\;\hat{\ell}_{tr}\;\;\hat{\ell}_{h'}\;\;\hat{j}_{h'} \\
& \sqrt{2}\;\;(-1)^{\Sigma}\hat{\Sigma}\;\;\frac{<\ell_{h'}0\ell_{tr}00|\ell_{p'}0>}{\sqrt{4\pi}}\;\left\{\begin{array}{ccc}\ell_{p'} & 1/2 & j_{p'}\\ \ell_{tr} & \Sigma & j_{tr}\\ \ell_{h'} & 1/2 & j_{h'}\end{array}\right\} \\
& <\Phi_{J_1}||[a^{+}_{j_{p'}}\tilde{a}_{j_{h'}}]_{j_{tr}}||\Phi_{J_2}> \\
& \int_0^{\infty}\mathcal{R}_{n_p\ell_{p'}j_{p'}}(r')V_{\ell_{tr},\,j_{tr}}(r,r')\mathcal{R}_{n_h\ell_{h'}j_{h'}}(r')\;dr'
\end{aligned} \tag{6}$$

A. form factor calculation in the case of phonon excitation

As it is well known, the coherent contributions of many p-h states is responsible for collective excitations of the core. The calculations of hole form factors performed with the QPM model take into account many multipole and spin-multipole excitations of the core [4,6].

If the coupling with one phonon state only is considered, the wave function of the excited core in Eq. 2 is described as a phonon of multipolarity ℓ_{tr}. Correspondingly, the coupling matrix element entering in the source term expression is given by Eq. 7.

$$i^{\ell_2-\ell_1} < \{[Y_{\ell_1}\chi_{1/2}]_{j_1}\Phi_{J_1}\}^M_J |H_{\rm int}| \{[Y_{\ell_2}\chi_{1/2}]_{j_2}\Phi_{J_2}\}^M_J >$$

$$= i^{\ell_2-\ell_{tr}-\ell_1}\ (-1)^{J-J_2-j_1-j_{tr}}\quad \hat{j}_{tr}\ \hat{j}_1\ \ \hat{j}_2\ \ \hat{\ell}_{tr}\ \hat{\ell}_2$$

$$W(j_2 J_2 j_1 J_1; J j_{tr})\hat{J}_1\ \sqrt{2}\ (-1)^{J_2+j_{tr}-J_1}\frac{<\ell_2 0 \ell_{tr}00|\ell_1 0>}{\sqrt{4\pi}}$$

$$\left\{\begin{array}{ccc} \ell_2 & 1/2 & j_2 \\ \ell_{tr} & 0 & j_{tr} \\ \ell_1 & 1/2 & j_1 \end{array}\right\} i^{\ell_{tr}}(-1)^{\ell_{tr}}\frac{dV(r)}{dr}$$

$$< \Phi_{J_1}||\alpha_{\ell_{tr}}||\Phi_{J_2} > \delta_{\ell_{tr} j_{tr}} \qquad (7)$$

It has been found in Ref. [4] that the inhomogeneous equation method predicts correct form factor shapes not only for fragments with small amplitudes but also for those with large amplitudes.

III. FORM FACTORS OF NEUTRON HOLE LEVELS IN ^{207}PB

A. Method and assumptions

In all the present calculations, the pure hole radial wave functions and separation energies were deduced using the Woods-Saxon potential previously used in QPM calculations [4,11].

The Serber-Exponential nucleon-nucleon interaction given in Ref. [8] was chosen for practical calculations of transition densities.

$$V = \left[{}^1V(r)\frac{1-\boldsymbol{\sigma}_1\cdot\boldsymbol{\sigma}_2}{4} + {}^3V(r)\frac{3+\boldsymbol{\sigma}_1\cdot\boldsymbol{\sigma}_2}{4}\right]\left(\frac{1+P_M}{2}\right)$$

Here P_M is the Majorana operator. The singlet and triplet potentials are given in Eq. 8

$${}^{1(3)}V(r) = -{}^{1(3)}V_0\ \exp(-{}^{1(3)}\mu r) \qquad (8)$$

with ${}^1V_0$= 108 MeV ${}^1\mu$= 1.409 fm^{-1}
${}^3V_0$= 193 MeV ${}^3\mu$= 1.506 fm^{-1}

Systematic calculations were performed assuming that the hole is coupled successively to each of the many 2h1p states which can be built taking into account all possible nn^{-1} and pp^{-1} particle-hole states up to a chosen maximum energy, with the coupled neutron hole spanning all possible sub shells. The separation energy and the spectroscopic strength of the two fragments in each independent calculation were deduced via a diagonalization procedure. Spectroscopic strength distribution resulting of the many independent calculations renormalized with the number of fragments are, as expected, much narrower than the more realistic QPM strength distribution of Ref. [11].

The computer code FFMIC [10] calculates in sequence the level source terms and form factors resulting of the coupling with each considered 2h1p state, using Eqs 4 and 3 respectively. The fragment with the smallest amplitude was selected in each case.

The form factor shapes, independently of the amplitudes, play a most important role in the determination of spectroscopic factors from transfer reaction cross sections. The deduced form factor radii together with the separation energies give a representative description of the fragment form factor shapes and were used in the discussion.

The distributions of form factor radii were fitted using a quadratic function of separation energy $R_{FF}=R_h + a_N\ (E_{sep}-E_h) + b_N\ (E_{sep}-E_h)^2$.

Here E_{sep} and E_h are the absolute values of the fragment and pure hole separation energies. R_{FF} and R_h are the fragment and pure hole form factor radii. a_N and b_N are the deduced parameters describing the radius linear and quadratic dependences respectively.

Relative spectroscopic strengths of the fragments located within separation energy sections were taken into account to obtain mean source terms and mean form factors as function of the section separation energy centroids. The distributions of the section form factor radii were fitted as for the individual levels, allowing the determination of the linear and quadratic dependence parameters a_S and b_S respectively.

B. Form factors and source terms of $g_{7/2}$ hole fragments

Particle-hole excitations up to E_x=15 MeV were taken into account in the performed calculations, the resulting fragments spanning a separation energy range from ~13 MeV up to ~30 MeV. The form factor shapes of the fragments exhausting the largest strength in each calculation involving one specific 2h1p configuration are nearly identical to the pure hole form factor shape. Only the form factors of the complementary fragments are discussed in the following. The overlap of such normalized form factors with the pure hole form factor was systematically calculated and all fragments with $\leq$ 90% overlap were

rejected. Their number amounts typically for 40% of the total but for few % only of the summed strength.

1. Dependence of source terms and form factors on the configurations

In the present schematic calculation, it is expected that the source terms, which involve the product of three hole or particle radial wave functions, would exhibit a large variety of radial shapes. This is shown in Fig. 1 for three levels resulting of the coupling with different 2h1p configurations located at similar separation energies.

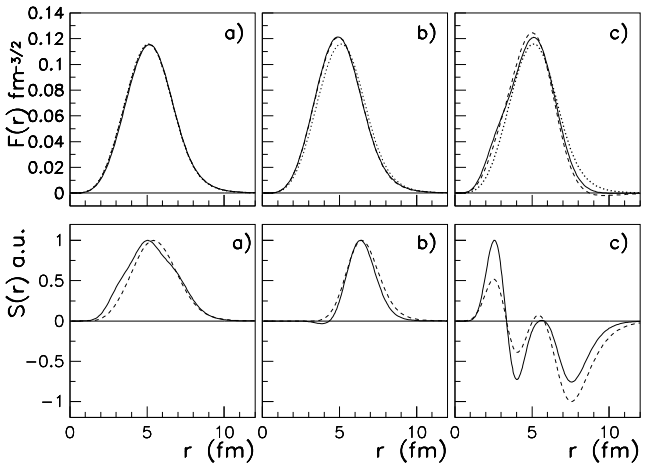

FIG. 1. Form factor and source term for three fragments $g_{7/2}$ at similar separation energy resulting of the coupling to different types of configurations. The solid and dashed curves are calculated with standard interaction range parameters and with two times smaller parameters respectively.The dotted curves are the pure $1g_{7/2}$ hole form factor. a) Configuration $(2d^n_{5/2}3p^{n\,-1}_{1/2})1h^{n\,-1}_{9/2}$ b) Configuration $(3d^{p\,-1}_{5/2}1i^p_{13/2})1i^{n\,-1}_{13/2}$ c) Configuration $(2f^{n\,-1}_{7/2}4s^n_{1/2})3p^{n\,-1}_{1/2}$.

It is striking that while the source term shape changes significantly or even strongly from one configuration to the other, this is not the case for the form factor. This may be related to the qualitative observation that all the three source terms become rather small at large radii (see Fig. 1), as discussed later on.

Form factor radii of the fragments built with nn^{-1} and pp^{-1} particle-hole excitations are compared in Fig. 2. The two distributions exhibit large fluctuations from level to level superimposed over a smooth increase with the separation energy reasonably described by a quadratic function. As shown in Table I, the fitting parameters a_N and b_N describing the relatively small radius linear and quadratic dependences on separation energy, and the full width at half-maximum of the radius distributions, are slightly larger in the case of nn^{-1} than for pp^{-1} excitations. This is also the case for the section parameters and widths.

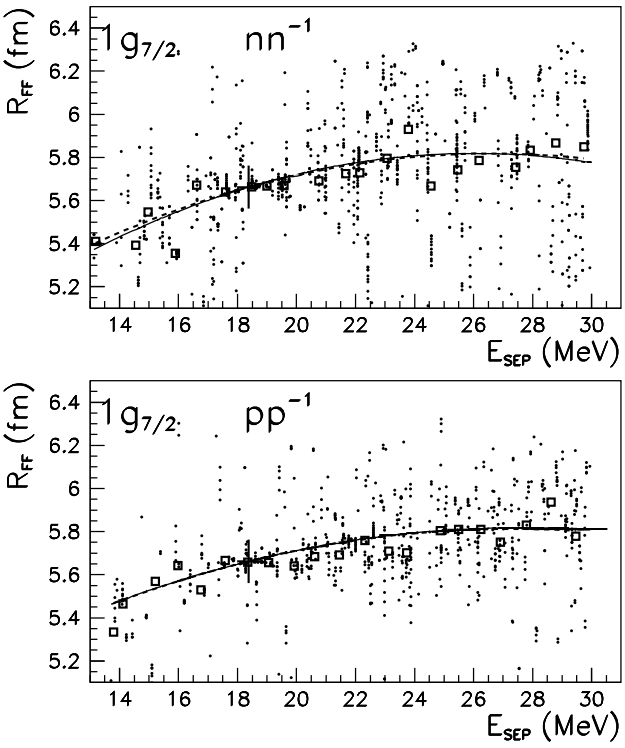

FIG. 2. Form factor radii of $g_{7/2}$ levels (dots) and 0.8 MeV wide groups of levels (squares) as function of separation energy absolute values. Large crosses: pure hole characteristics. Full lines and dashed lines : fits to the level and section radius distributions respectively. Upper figure: levels built with nn^{-1} particle-hole configurations. Lower figure: with pp^{-1} configurations.

2. Strength dependence of the fragment form factor radii

The radius distribution corresponding to all accepted fragments is shown in Fig. 3a, together with the corresponding fits. The strength of such levels resulting of the hole coupling with pure 2h1p configurations drops very rapidly on both side of the pure hole separation energy. Radius distributions obtained by selecting only the levels with maximum strength or the levels with minimum strength in 0.8 MeV wide adjacent sections are shown in Fig. 3b. The fitting parameters and distribution widths are compared in Table I. It is found that the distributions do not depend much on the strength selection, but for the smaller width observed for the levels with the larger strengths. It is thus expected, as shown in Fig. 2, Fig. 3a and Table I, that the section radius distributions exhibit similar behaviors and similar fitting parameters as the level distributions. The weighted average performed to

get the mean form factors obviously reduces the distribution widths.

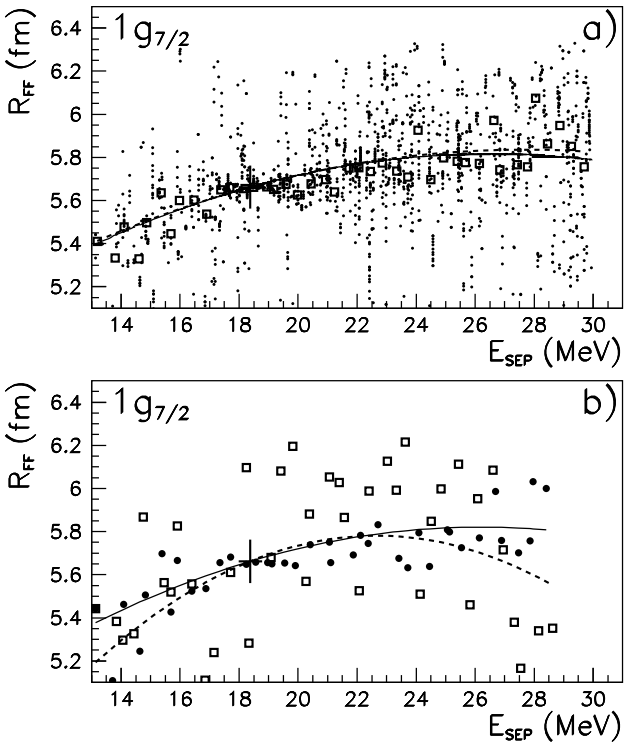

FIG. 3. Comparison of radius distributions for different conditions on the level strengths. Large crosses, full and dashed lines as in Fig. 2. a) Level form factor radii (dots) and 0.4 MeV section mean radii (squares) without strength selection. b) dots: radius distribution for the levels exhausting the maximum strength in each 0.75 MeV section. Squares: radius distribution for the levels exhausting the minimum strength in each 0.75 MeV section (see text).

Among all fragments, those with $\geq$1% strength are found within $\sim \pm$ 1 MeV around the pure hole separation energy. Fig. 4 presents the distributions of form factor radii in the above separation energy range obtained for the fragments with $\geq$1% strength (group 1) and $\leq$1% strength (group 2). The fitting parameters and widths are given in Table I. The radius distribution widths of the level and sections are much smaller for both groups (especially for group 1) than observed for all fragments in the total separation energy range. The linear dependence parameters of the group 1 and group 2 level radii drop to ~20% and ~30% respectively of the value deduced for all fragments in the full separation energy range.

In their analysis of their $(e,e'p)$ experiments, Den Herder et al [12] have assumed that form factor radii of proton inner hole states spread by their coupling with other configurations would not change with separation energy.

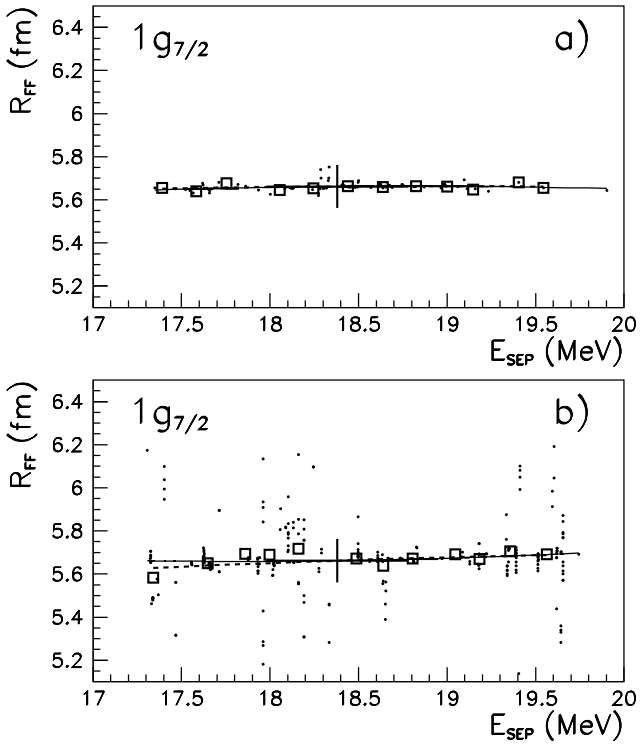

FIG. 4. Form factor radii of $g_{7/2}$ levels (dots) and 0.2 MeV wide sections (squares). Large crosses, full and dashed lines as in Fig. 2. a) Levels with individual strengths $\geq$0.01. b) Levels with individual strengths $\leq$0.01 (see text).

TABLE I. Characteristics of $g_{7/2}$ form factor radii. a_N, a_S and and b_N, b_S are the parameters describing the linear and quadratic dependence of the level radii and the section mean radii on separation energy absolute value. $Fwhm_N$ and $Fwhm_S$ are the full width at half-maximum of the level and section radius distributions respectively.

levels	a_N	a_S	b_N	b_S	$Fwhm_N$	$Fwhm_S$
	fm MeV^{-1}		fm MeV^{-2}		fm	fm
nn^{-1}	0.041	0.038	-0.003	-0.0023	0.56	0.17
pp^{-1}	0.034	0.034	-0.002	-0.0019	0.45	0.14
all	0.038	0.037	-0.0023	-0.0020	0.51	0.19
[a]	0.041		-0.0026		0.26	
[b]	0.056		-0.0065		0.66	
1 [c]	0.0069	0.0053	-0.0086	-0.0047	0.044	0.026
2 [d]	0.012	0.028	-0.010	-0.0047	0.152	0.072

[a] Selection of the fragment with maximum strength in each 0.8 MeV wide sections

[b] Selection of the fragment with minimum strength in each 0.8 MeV wide sections

[c] fragments with $\geq$0.01 strength in each calculation

[d] Fragments spanning the same separation energy range as group 1, but with $\leq$0.01 strength.

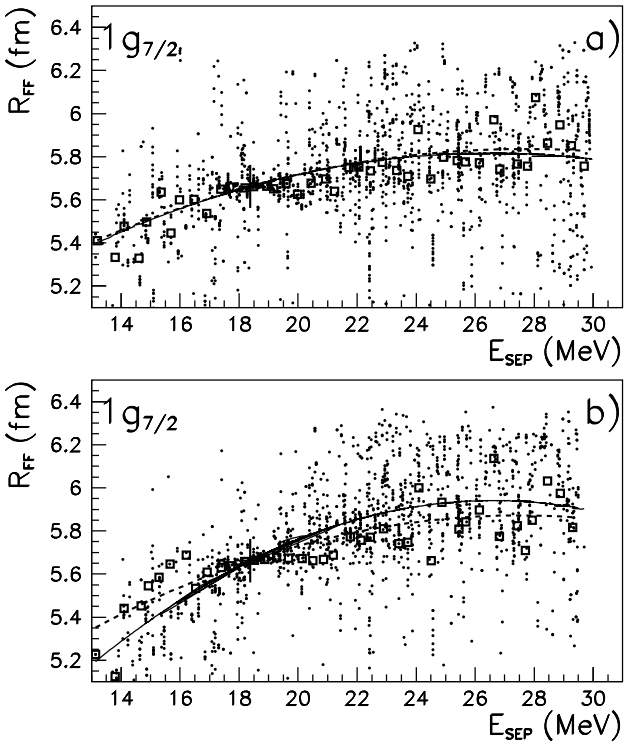

FIG. 5. Form factor radii of $g_{7/2}$ levels (dots) and 0.4 MeV wide sections (squares). large crosses, full and dashed lines as in Fig. 2. a) Results obtained with standard range parameters. b) Results obtained with two times smaller range parameters.

The present calculations, show that this assumption is indeed qualitatively supported in the framework of incoherent underlying core excitations, but only over the small separation energy range where the strength is expected to be significantly spread.

TABLE II. Variation with the interaction range of the separation energy absolute value E_{SEP} and form factor radius R_{FF} for three $g_{7/2}$ levels with different configurations

configuration	a) [a]	b) [b]	c) [c]
E_{SEP} (MeV) [d]	16.320	16.198	16.462
E_{SEP} (MeV) [e]	16.298	16.193	16.462
R_{FF} fm [d]	5.695	5.482	5.475
R_{FF} fm [e]	5.674	5.489	5.462

[a] a) $(3p^{n\,-1}_{1/2}\,2d^{n}_{5/2})1h^{n\,-1}_{9/2}$ j=2

[b] b) $(3d^{p\,-1}_{5/2}\,1i^{p}_{13/2})1i^{n\,-1}_{13/2}$ j=4

[c] c) $(2f^{n\,-1}_{7/2}\,4s^{n}_{1/2})3p^{n\,-1}_{1/2}$ j=4

[d] with standard interaction parameters

[e] with half values of the standard interaction parameters

3. Dependence on the interaction range parameters

An increase of the singlet and triplet potentials by a factor of 2 was found to have negligible effect on the calculated form factor shapes and form factor radii.

Systematic calculations were performed in more details with two times smaller range parameters than given in Ref. [8] for comparison with the standard calculations. The form factor and source term shapes obtained with the reduced parameters for the configurations discussed in Sect. III B 1 are compared with the standard results in Fig. 1.

For all three configurations, the dependence on the range parameters of the form factors is obviously much smaller than the corresponding source term one. The dependence on the range parameters of the separation energy and form factor radius is quite negligible in the three cases, as shown in Table II.

The distributions of level and section form factor radii obtained with the standard range parameters and the modified ones are compared in Fig. 5, together with the corresponding fitting curves. The distribution of the section form factor radii changes somewhat less with the interaction range than that of individual levels. The section linear and quadratic parameters increase only by ∼20%, compared with ∼50% for the level fitting parameters, as shown in Table III.

Mean source terms and mean form factors deduced for three separation energy groups, using standard or reduced range parameters are compared in Fig. 6. The observed dependence of the mean form factor shapes on the range parameters is found even smaller than in the case of individual levels.

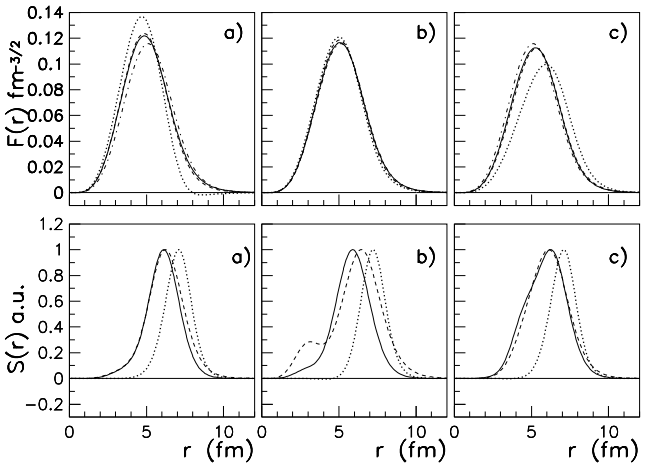

FIG. 6. Mean form factors and mean source terms for three $g_{7/2}$ separation energy groups. Solid and dashed curves: with standard and two times smaller interaction range parameters respectively. Dotted curves: QPMFF results. Dashed-dotted curves: pure hole form factor. a) 13.0-14.5 MeV. b) 16.0-17.5 MeV. c) 25.0-26.5 MeV.

4. Comparison with QPM calculations

The present $g_{7/2}$ radius distribution is compared in Fig. 7 with the distribution obtained in the framework of the QPM model (hereafter QPMFF form factor) following the method of Ref. [4]. The two distributions are strikingly different, with a much larger increase of QPMFF radii with separation energy.

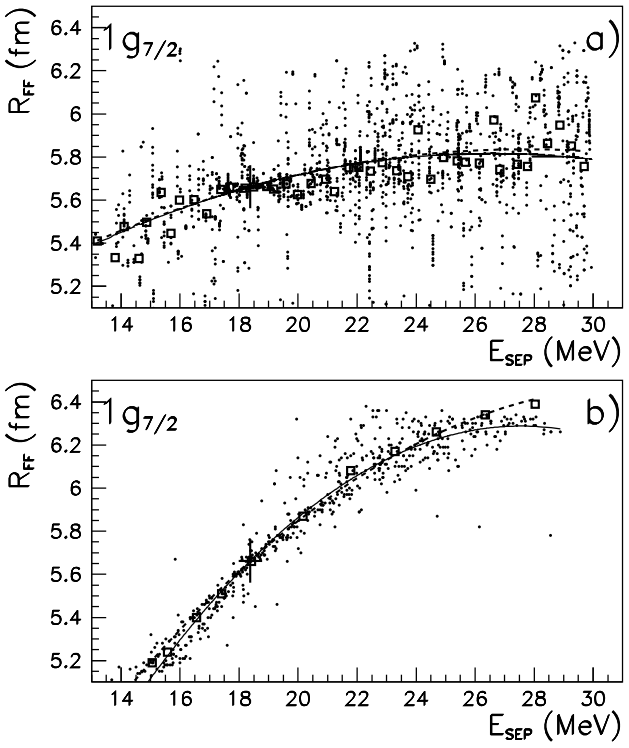

FIG. 7. Comparison of the $g_{7/2}$ radius distributions with previous QPMFF results. Large crosses, full and dashed lines as in Fig. 2. a) Present calculation. b) QPMFF predictions.

TABLE III. Characteristics of $g_{7/2}$ form factor radii as function of the interaction range and comparison with QPMFF calculations. a_N, a_S, b_N, b_S, $Fwhm_N$ and $Fwhm_S$ as in Table(1).

	a_N	a_S	b_N	b_S	$Fwhm_N$	$Fwhm_S$
	fm MeV^{-1}		fm MeV^{-2}		fm	fm
all	0.038	0.037	-0.0023	-0.0020	0.51	0.19
all [a]	0.068	0.045	-0.0041	-0.0025	0.47	0.23
QPMFF [b]	0.136	0.123	-0.007	-0.0047	0.23	0.066

[a] Fragment radii calculated with half the standard range parameters

[b] For g7/2 groups of levels calculated in the framework of the QPM model.

The QPMFF radius distributions of both the levels and sections are characterized by much larger values of the fitting parameters (see Table III), especially for parameter a describing the linear dependence with separation energy. The QPMFF radius distributions widths are typically 50% of the present calculated widths.

As discussed in Ref. [4], the large dependence of QPMFF form factor radii on separation energy is related to the surface localization of the corresponding source terms, itself governed by the radial shape of phonon excitation transition densities. The expected very different radial shapes of transition densities obtained for pure particle-hole excitations compared with the Woods-Saxon derivative shape entering QPM calculations is illustrated in Fig. 8 for several levels with rather large relative strengths, sampling different separation energy ranges. The microscopic transition densities contribute at much smaller radial values than the QPM transition densities.

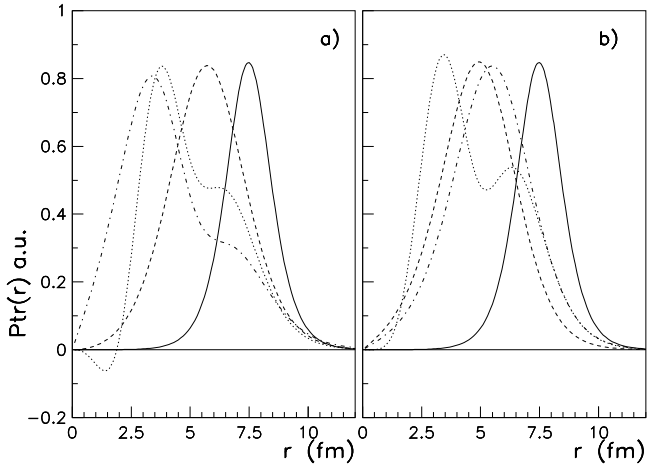

FIG. 8. Comparison of transition probabilities involved in a few levels with the largest strengths in different separation energy ranges, with the transition radial shape of QPMFF calculations shown as full lines. a) E_{SEP}=14.83, 15.38, 18.57 MeV: dashed, dotted and dashed-dotted lines respectively. b) E_{SEP}=19.11, 21.10, 23.41 MeV: dashed, dotted and dashed-dotted lines respectively.

The QPMFF mean source terms and mean form factors deduced for three separation energy sections are shown in Fig. 6 together with the results obtained in the present calculations at similar separation energies.

The QPMFF mean source terms do not depend much of the section chosen. They result not only of many level contributions, but for each of them of coherent contributions of many coupling channels. In the present calculation, the summation of individual level terms weighted by the corresponding relative strengths lead to section source terms which detailed shape change with the section, the position of the maximum remaining however ~1 to 1.5 fm inside the QPMFF ones. This behavior

is responsible for the observed smaller variation of form factor radii with separation energy.

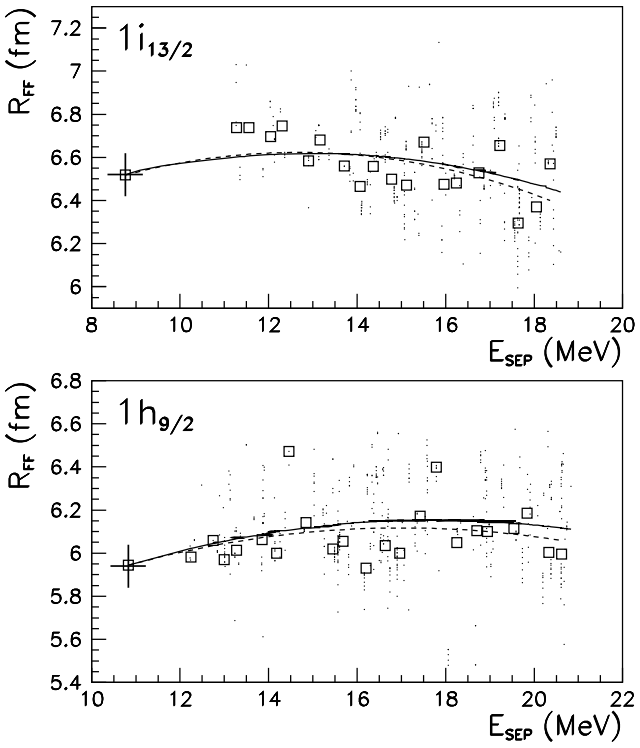

FIG. 9. Form factor radii of $i_{13/2}$ and $h_{9/2}$ neutron hole levels (dots) and 0.4 MeV wide sections (squares).Large crosses, full and dashed lines as in Fig. 2.

C. Form factor radius distributions of valence and inner hole levels and sections

$i_{13/2}$, $h_{9/2}$ and $h_{11/2}$, $g_{9/2}$ form factor radii of the levels resulting from the hole coupling with independent 2h1p configurations are shown in Fig. 9 and Fig. 10 respectively. All distributions exhibit large fluctuations from level to level superimposed over a smooth dependence with the separation energy reasonably described by a quadratic function.

TABLE IV. Characteristics of neutron hole form factor radii. a_S and b_S are the fitting parameters describing the section mean radii and $Fwhm_S$ the full widths at half-maximum. a_{SQ} and b_{SQ} are the fitting parameters given for QPMFF calculations.

holes	E_{SEP} MeV	R_{FF} fm	a_S fm	a_SQ MeV^{-1}	b_SQ fm	b_SQ MeV^{-2}	$Fwhm_S$ fm
$i_{13/2}$	8.75	6.52	0.054	0.079	-0.007	-0.005	0.35
$h_{9/2}$	10.83	5.95	0.056	0.137	-0.0045	-0.007	0.29
$h_{11/2}$	15.45	6.23	0.044	0.091	-0.0051	-0.004	0.18
$g_{7/2}$	18.38	5.66	0.037	0.124	-0.0020	-0.004	0.19
$g_{9/2}$	21.40	5.92	0.021		-0.0016		0.15

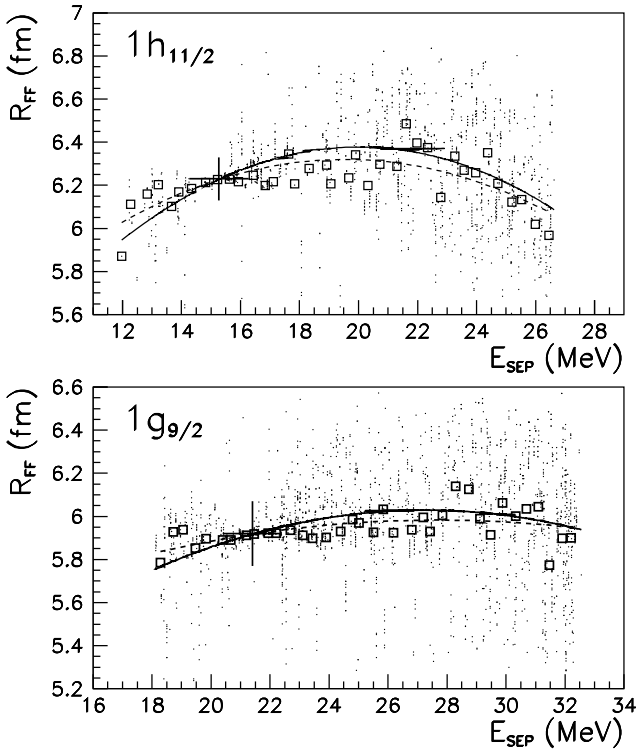

FIG. 10. Form factor radii of $h_{11/2}$ and $g_{9/2}$ neutron hole levels (dots) and 0.4 MeV wide sections (squares). Large crosses, full and dashed lines as in Fig. 2.

The same trend, with smaller fluctuations, is observed for energy section results.

The characteristics of the section form factor radii deduced of the present calculations are summarized in Table IV for the different hole states. The fitting parameters describing the linear and quadratic dependence are compared with those previously obtained in Ref. [4]. Parameter values describing the linear radius increase with separation energy are reduced to 68%, 40%, 48% and 30% of the values deduced with the QPMFF calculations for the $i_{13/2}$, $h_{9/2}$, $h_{11/2}$ and $g_{7/2}$ hole sections respectively.

IV. FORM FACTORS AND SPECTROSCOPIC FACTOR ANALYSIS IN THE $(\vec{D},T)$ REACTION AT 200 MEV

In a first approximation, one may assume that the (d,t) differential cross section per nucleon of each level within a given separation energy section depends linearly on the corresponding form factor radius. Under this condition, the cross section summed over the individual levels in a section is well approximated by the cross section calculated with the normalized mean form factor and the summed spectroscopic factors in the section. This assumption has been successfully checked [4] by comparing the predicted sum of individual cross sections of QPMFF levels with the corresponding total section cross section.

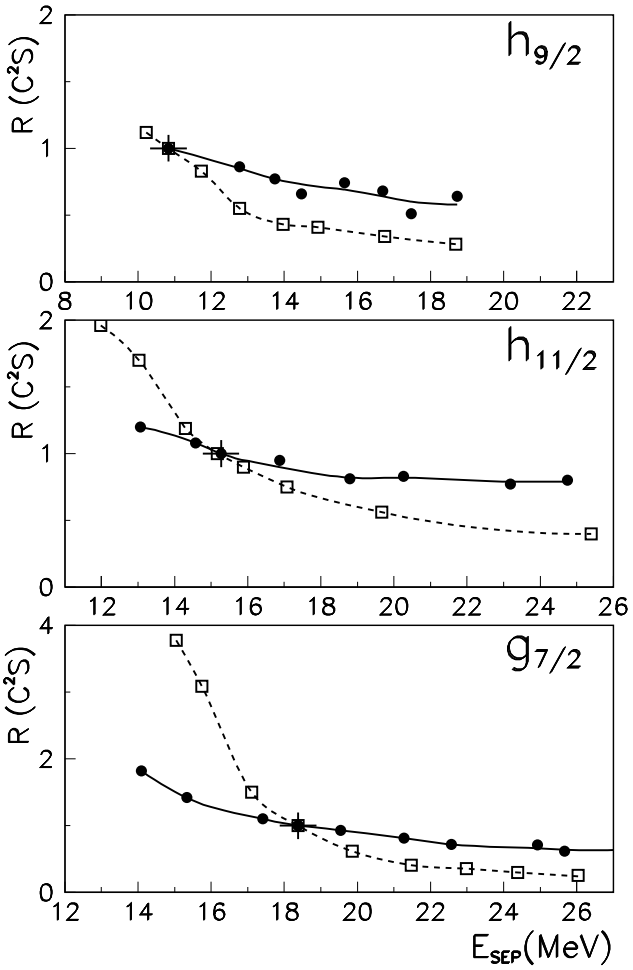

FIG. 11. Ratio R_{C^2S} of model dependent and standard spectroscopic factors (see text). Full and broken lines: mean results of present and QPMFF calculations respectively. Full circle and empty squares indicate the section mean separation energies and mean radii in the present and the QPMFF calculations respectively.

DWBA differential cross sections and analyzing powers of the $^{208}Pb(\vec{d},t)^{207}$ reaction at E_d=200 MeV were obtained under those conditions for different $h_{9/2}$, $h_{11/2}$ and $g_{7/2}$ sections using mean form factors corresponding to the present calculations. As observed in Ref. [4], the angular distribution shapes remain rather stable within few MeV below and several MeV beyond each pure hole separation energy.

Ratio R_{C^2S} of spectroscopic factors of interest to standard spectroscopic factors obtained assuming no dependence of DWBA observables with separation energy were determined in the corresponding energy ranges. They are shown in Fig. 11, together with the ratio previously obtained in QPMFF calculations. The correction factors R_{C^2S} are found much nearer to 1 in the present calculations than for QPMFF calculations, as expected from the weaker dependence of form factor radii.

V. SUMMARY AND DISCUSSION

We have used the inhomogeneous equation method to calculate form factors of fragmented neutron hole states in ^{207}Pb resulting of the hole coupling to incoherent 2h1p states. Amplitudes of the wave function component with no excitation of the core and source terms were calculated using the Serber-exponential nucleon nucleon interaction of Ref. [8].

The behavior of the section and level form factors has been studied in detail in the case of the $g_{7/2}$ hole states. The form factor shapes are found to change much less than the corresponding source term shapes with the chosen 2h1p configurations. Form factor radii exhibit large fluctuations from level to level, superimposed over a smooth increase with separation energy which is fitted by a quadratic function. The overall behaviors of radius distributions obtained for configurations built with nn^{-1} or pp^{-1} ph excitations differ only slightly and no significant role of level amplitudes is found. The level form factor shapes are nearly insensitive to the chosen interaction strength. The dependence on the interaction range is significant, but relatively weak with typically 20% increase of linear radius dependence on separation energy for two times smaller range parameters.

Form factor radius distributions of $i_{13/2}$, $h_{9/2}$, $h_{11/2}$ and $g_{9/2}$ levels exhibit similar characteristics. The parameters describing the linear radius increase with separation energy are found always smaller than in previous QPMFF calculations. Spectroscopic factors extracted via a DWBA analysis of the $(\vec{d},t)$ reaction at E_d=200 MeV depend sensitively of the assumed form factor shapes. The present calculations based on the schematic (and unrealistic assumption) of incoherent p-h excitation of the core via a nucleon nucleon simple interaction lead to ratio of spectroscopic factor to standard ones much nearer to 1 than found under the assumption of collective coupling, located at the surface.

Den Herder et al [12] have used form factor radii independent on separation energy in their analysis of proton hole states studied via the $(e,e'p)$ reaction. This assumption would be qualitatively supported in the case of incoherent excitations over only typically 2 MeV around the pure hole separation energy. Much larger radius increase with separation energy are expected if the fragmentation involves surface vibrations, as described in QPMFF calculations [4]. The correction induced in $(e,e'p)$ analysis may be however estimated the order of 10 times smaller than found in the above discussed (d,t) reaction analysis.